

Fingerprints of classical chaos in manipulation of cold atoms in the dynamical tunneling experiments

Shmuel Osovski and Nimrod Moiseyev

Department of Chemistry and Minerva Center of Nonlinear Physics in Complex Systems Technion, Israel Institute of Technology, Haifa 32000, Israel

(Received 28 March 2005; revised manuscript received 7 June 2005; published 7 September 2005)

The recent pioneering experiments of the [Nature **412**, 52 (2001)] and [Science, **293**, 274 (2001)] groups have demonstrated the dynamical tunneling of cold atoms interacting with standing electromagnetic waves. It has been shown [Phys. Rev. Lett. **89**, 253201 (2002)], that the tunneling oscillations observed in these experiments correspondingly stems from two- and three-Floquet quantum state mechanism and can be controlled by varying the experimental parameters. The question where are the fingerprints of the classical chaotic dynamics in a quantum dynamical process which is controlled by 2 or 3 quantum states remains open. Our calculations show that although the effective \hbar associated with the two experiments is large, and the quantum system is far from its semiclassical limit, the quantum Floquet-Bloch quasienergy states still can be classified as regular and chaotic states. In both experiments the quantum and the classical phase-space entropies are quite similar, although the classical phase space is a mixed regular-chaotic space. It is also shown that as the wave packet which is initially localized at one of the two inner regular islands oscillates between them through the chaotic sea, it accumulates a random phase which causes the decay of the amplitude of the oscillating mean momentum, $\langle P(t) \rangle$, as measured in both experiments. The extremely high sensitivity of the rate of decay of the oscillations of $\langle P(t) \rangle$ to the very small changes in the population of different Floquet-Bloch states, is another type of fingerprint of chaos in quantum dynamics that presumably was measured in the NIST and AUSTIN experiments for the first time.

DOI: [10.1103/PhysRevA.72.033603](https://doi.org/10.1103/PhysRevA.72.033603)

PACS number(s): 03.75.Kk

I. INTRODUCTION: MANIPULATIONS OF COLD ATOMS IN THE NIST AND AUSTIN EXPERIMENTS

Experiments done in recent years by the Phillips group in NIST [1] and the Raizen group in AUSTIN [2,3] have demonstrated dynamical tunneling of cold atoms in a 1D optical lattice. In the NIST experiment a Bose-Einstein condensate of sodium atoms was prepared in a magnetic trap. By turning on adiabatically a one-dimensional standing wave more than 99% of the sodium atoms were loaded into the bottom of the lowest Bloch band (associated with quasimomentum equal to zero, $\hbar k=0$) of the one-dimensional optical lattice. The atoms were driven by a time periodic field which was induced by the modulated standing wave. By a sudden shift of the position of the standing wave the wave packet was transferred to the selected region in the classical phase space. After the atoms have interacted with the modulated standing wave for a selected number of modulation periods, the standing wave is turned off. Shortly later the atomic momentum distribution was measured.

In the AUSTIN experiment the cesium atoms were first cooled and trapped in a magneto-optic trap. After further cooling they were stored in a linearly polarized optical lattice. The optical lattice has been ramped adiabatically to localize the atoms in the potential wells. The lattice has been then suddenly spatially shifted to prepare a localized atomic wave packet centered at the selected region in the classical phase space. After the state preparation, the atoms were subjected to a time-periodic interaction for a selected number of modulation periods. The atoms were then allowed to expand freely for 20 ms, after which the atomic momentum distribution was measured.

In both experiments the light was detuned far from the atomic resonances. The negligible population of the first excited electronic state enables one to describe the atoms in a standing wave with time periodic amplitude modulation, by a time periodic one-dimensional center-of-mass model Hamiltonian [5]. In both cases the corresponding classical Poincaré surface of sections for position, q , and momentum, p , in an amplitude-modulated optical lattice, consist of a bounded chaotic sea. In both cases regular islands centered at $q=0$ and $p=\pm p_0$ (see Figs. 1 and 2) are embedded inside the bounded chaotic sea. In both cases the initial wave packet of the cold

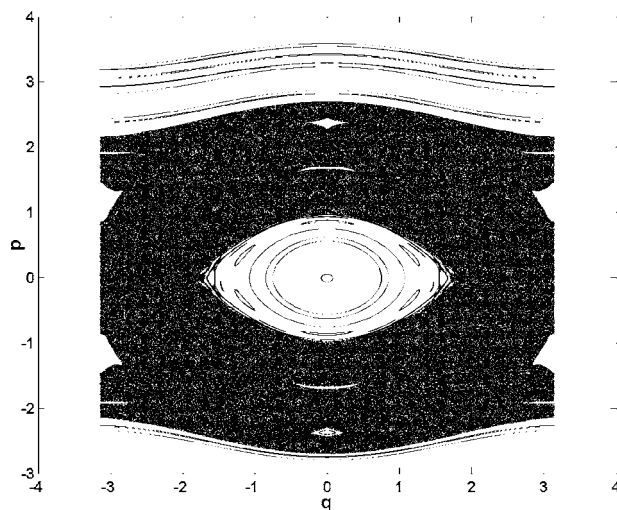


FIG. 1. The stroboscopic Poincaré section of the classical phase space for the NIST experiment.

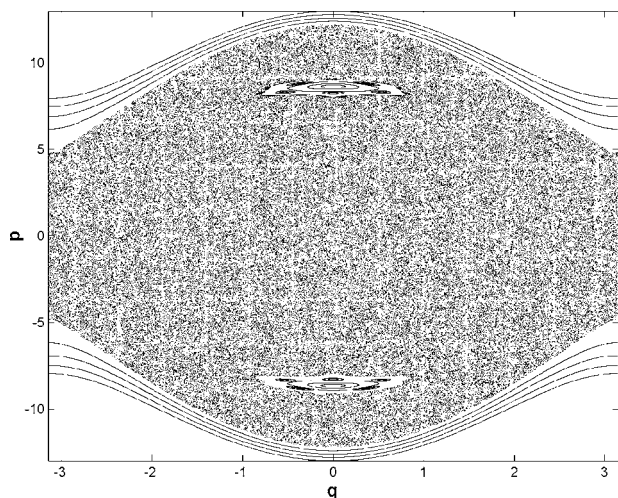


FIG. 2. The stroboscopic Poincaré section of the classical phase space for the AUSTIN experiment.

atoms was localized at one of these two mirror reflected regular inner islands. In both cases the measured atomic momentum distributions exhibit oscillations which were associated with the dynamical tunneling of the cold atoms through the chaotic sea, from one regular inner island to the other.

A comparison between Figs. 1 and 2 with Fig. 1 in Ref. [4] shows that the stroboscopic synoptic Poincaré section of classical phase space for the NIST and AUSTIN experiments and the Poincaré surface of section as obtained for a driven rotor, are very much alike. In their theoretical studies of a continuously driven rotor, Averbukh *et al.* [4] were first to show that for sufficiently small value of \hbar , a dynamical tunneling through a chaotic region is obtained. They have shown that the interaction with the time periodic field changes the hindered rotational motion from anticlockwise to clockwise (hindered) rotational motion. As it was indicated before in Ref. [4] this transition is classically forbidden and is another example of a quantum mechanical tunneling phenomenon occurring due to the time-reversal symmetry of the Hamiltonian. It is very tempting to conclude that these classically forbidden transitions have been measured in the NIST and AUSTIN experiments. However, in both NIST and AUSTIN experiments the effective Planck constants are much larger than the area of the inner regular islands [6]. *Therefore, in both cases the regular inner islands do not support even a single quantum state and the dynamics of the driven atoms in the one-dimensional oscillating space and time potentials is far from its classical limit.* In both cases by varying the experimental parameters which are associated with the effective Planck constant, the oscillations of the mean momentum can be enhanced by several orders of magnitude or completely suppressed [6].

The open question we wish to answer in this paper, is whether there are fingerprints of the classical mixed (regular-chaotic) phase space in the quantum dynamics although the effective Planck constant is large.

In the next section we will show that in spite of the large value of effective \hbar still the Floquet-Bloch quasienergy states can be classified as regular and chaotic states. Husimi distributions of the quasienergy Floquet-Bloch states show that

the regular quasienergy states are exponentially localized at the regular islands. This is not a surprising result since it is well known that quantum wave packets are localized even at unstable hyperbolic fixed points in the classical phase space [7,8]. The classification of quantum regular and chaotic quasienergy states is obtained by the calculations of the Shannon entropy and the mean energy of the field-free Hamiltonian, $\langle H_0 \rangle$ as first proposed in Ref. [9]. The definition of entropy in information theory is the Shannon entropy. See, for example, a review on the general properties of entropy in Ref. [10]. The chaotic states are associated with quasienergy Floquet-Bloch states which all provide about the same value of $\langle H_0 \rangle$ and about the same maximal value of the Shannon entropy, $\langle S \rangle$. As we show in Sec. II due to the large effective Planck constants in the NIST experiments the two regular quasienergy Floquet-Bloch states which are associated with the inner regular islands embedded inside the chaotic sea, are “pushed” into the chaotic region in the $\langle H_0 \rangle$ vs $\langle S \rangle$ plot, but still are (somehow) separated from the chaotic states. In the AUSTIN experiment the situation is more complicated. One of the two regular quasienergy Floquet-Bloch states interferes with a chaotic state. This kind of interference gives rise to the 3-state dynamical mechanism in the AUSTIN experiment [6]. The enhancement of tunneling through a 3-state mechanism first studied for a tunneling through a static potential barrier. See the study of Hänggi and co-workers of coherent and incoherent chaotic tunneling near singlet-double crossings [11] and the study of Vorobeichik and his co-workers for the study of exchange of power between two identical coupled waveguides with embedded periodic structure along the propagation axis [12]. Note that within the framework of the paraxial approximation the Hamiltonian of the two-coupled waveguide is an equivalent problem to the one studied in Ref. [11] when a weak laser field rather than a high intensity one is used.

In Sec. III, we calculate the Mirbach-Korsch quantum phase-space entropy [13] to the NIST and AUSTIN experiments. A comparison between the quantum and the classical phase-space entropies clearly shows the fingerprints of the mixed (regular-chaotic) structure of the classical phase space in the quantum systems of continuously driven cold atoms.

In Sec. IV, we present the Husimi representation of the inner-regular, outer-regular, and chaotic quasienergy states as classified in Sec. II. The Husimi representation of the inner-regular quasienergy states are slightly different from those calculated before in Ref. [14] due to our use of different definition for the Husimi representation of quasienergy states (we took into consideration the spatial periodic behavior of the potential). This is however a minor point in our motivation to represent the Husimi distributions. We clearly show in this section the one-to-one correspondence between the quasienergy states as calculated for the NIST and AUSTIN experiments and the mixed regular-chaotic structure of the classical phase space. We also show how in the AUSTIN experiment the linear combinations of the three quasienergy Floquet-Bloch states that control the dynamics provide a wave packet which is exponentially localized and is centered at the middle of one of the two mirror-reflected regular islands embedded inside the chaotic sea.

In Sec. V the effect of the band structure of the Floquet-Bloch quasienergy spectrum on the decay of the amplitude of the oscillating measured mean momentum distribution in the NIST and AUSTIN experiments is studied. We show that the oscillations in the mean momentum of the periodically driven cold atoms in the one-dimensional optical lattice, appear if and only if the $k=0$ Bloch quasimomentum state is populated by more than 99%. This result is in a complete harmony with the experimental observation [1]. The question is, why the oscillatory behavior of the mean momentum is so sensitive to the population of the $k=0$ Bloch quasimomentum state? As we show here it is due to the random phase distribution of the population probability amplitudes of the $k \neq 0$ Bloch quasimomentum states by the initial wave packet. The averaging over components with a random phase distribution leads to the suppression of the oscillations of the mean momentum. As it is shown here the high sensitivity of the rate of decay of the oscillations due to the very small changes in initial wave packet are in a way, a fingerprint of the classical chaos in quantum mechanical dynamical process.

II. REGULAR AND CHAOTIC FLOQUET-BLOCH QUASIENERGY STATES ASSOCIATED WITH THE MANIPULATION OF COLD ATOM EXPERIMENTS

Let us first briefly describe how the Hamiltonian is derived. For a detailed derivation of the model Hamiltonian see, for example, Ref. [5]. The laser frequency, ω_L , was chosen to be detuned from the atomic frequency, ω_a . The detuning parameter is given by $\delta_L = \omega_L - \omega_a$. The laser field is sufficiently weak to justify a construction of a field free Hamiltonian which consists of two electronic states. The ground state and the first excited electronic state. Since the coupling between the center of mass of the atom and the relative (\sim electronic) coordinates is induced by a linearly polarized light (the light is propagated along the x direction) the field-free Hamiltonian is given by

$$H_0 = \frac{p_x^2}{2M} (|e\rangle\langle e| + |g\rangle\langle g|) + \hbar \omega_a |e\rangle\langle e| + 0 |g\rangle\langle g|. \quad (1)$$

The standing laser field couples the two electronic states. The standing laser wave is composed of two running waves, $E_0[\cos(\omega_L t - k_L x) + \cos(\omega_L t + k_L x)]/2 = E_0 \cos(\omega_L t) \cos(k_L x)$. Within the framework of the dipole approximation the coupling term is given by

$$V_{\text{coupling}} = dE_0 \cos(\omega_L t) \cos(k_L x) (|e\rangle\langle g| + |g\rangle\langle e|), \quad (2)$$

where E_0 is the maximum field amplitude, $k_L = 2\pi/\lambda$, $\lambda = c/\omega_L$ is the wavelength of the laser light beam, and the dipole transition matrix elements, d , is given by

$$d = \langle g | \hat{z}_{\text{elec}} | e \rangle. \quad (3)$$

The atoms are trapped in a one-dimensional optical lattice when a standing laser wave is used. In the NIST and AUSTIN experiments the atoms in the one-dimensional optical lattice were driven by the use of two-standing laser waves. The maximum field amplitudes of the standing waves

are denoted by $E_{\pm} = E_0 \pm \delta E_0$, the corresponding frequencies are given by $\omega_{\pm} = \omega_L \pm \delta\omega$. The Rabi frequency for each of the waves is given by

$$\Omega_{\pm} = \frac{dE_{\pm}}{\hbar}. \quad (4)$$

Under the assumption that the linear polarized light induced the 1D center of mass motion of the atoms, and by using the two-electronic state approximation within the framework of the dipole approximation, and under the assumption of a one photon absorption process, the time dependent solution of the Schrödinger equation is given by

$$\Psi = \chi_g(x, t) |g\rangle + \chi_e(x, t) |e\rangle e^{-i\omega_L t}. \quad (5)$$

The center of mass Hamiltonian is obtained under three more assumptions, (1) rotating wave approximation [i.e., $\exp(i\omega_L t) \cos(\omega_{\pm}) \sim 0.5 \exp(\pm i0.5\delta\omega t)$]; (2) atoms move slowly and $k_{\pm} \equiv 2\pi\omega_{\pm}/c \sim k_L \equiv 2\pi\omega_L/c$ where k_L is the mean wave vector of the two standing waves; (3) the detuning frequency $\delta_L = \omega_{\text{atom}} - \omega_L$ should be sufficiently large such that the population of the excited electronic state is negligible. Under these approximations the center of mass Hamiltonian is given by

$$H = \frac{p_x^2}{2} + V_0 \cos(2k_L x) + V_1 \cos(2k_L x) \cos(\delta\omega t), \quad (6)$$

where

$$V_0 = \frac{\hbar(\Omega_+^2 + \Omega_-^2)}{16\delta_L} \quad (7)$$

and

$$V_1 = \frac{\hbar\Omega_+\Omega_-}{8\delta_L}. \quad (8)$$

The period of the modulations is given by

$$T = \frac{2\pi}{\delta\omega}. \quad (9)$$

Equation (6) is reduced to dimensionless effective Hamiltonian which is given by

$$H_{\text{eff}}(q, t) = \frac{p^2}{2} - \gamma[\theta + \cos(\omega t)] \cos(q), \quad (10)$$

where $\gamma = 4k_L^2 \delta\omega V_0/M$ and $\theta = (\Omega_+/\Omega_+ \Omega_- - \Omega_+)/2$. Note that from now on t and q are the dimensionless scaled time and coordinate correspondingly. In Ref. [1] where the NIST experiment is presented, a transformed Hamiltonian was used rather than the one given in Eq. (10). Let $\Phi(t)$ be the solution of the time dependent Schrödinger equation with the Hamiltonian given in Eq. (10),

$$H_{\text{eff}}\Phi(t) = i\hbar_{\text{eff}} \frac{\partial}{\partial t} \Phi(t) \quad (11)$$

and Ψ_{NIST} be the solution of the Hamiltonian given in Ref. [1] then,

$$\Psi_{\text{NIST}} = e^{-i(\kappa/\hbar_{\text{eff}})[r-(2\varepsilon/w)\cos(q)]}\Phi(t), \quad (12)$$

Using the transformation presented in Eq. (11) the NIST parameters were calculated, and are given by $\gamma=2\varepsilon\kappa=0.9628$ and $\theta=1/2\varepsilon=1.724$. For the AUSTIN experiment

$$\Psi_{\text{AUSTIN}} = \Phi(t), \quad (13)$$

where $\Phi(t)$ is the solution of the time dependent Schrödinger equation with the Hamiltonian given in Eq. (10) when the dimensionless parameters are given by $\gamma=10.5$ and $\theta=1$.

The stroboscopic Poincaré section of the classical phase space presented in Figs. 1 and 2 was obtained by solving the Hamilton equations of motion for the AUSTIN and NIST experimental parameters. The classical Hamiltonian is as defined in Eq. (10) where p is the classical momentum. The Poincaré surface of section is plotted every time period ($t=nT$) where in our scaled units $T=1$ for the AUSTIN parameters and $T=2\pi$ for the NIST experiment. These values for T were chosen to keep the same units as in our previous calculations presented in Ref. [6]. Three types of motion are observed in the classical phase space,

(1) chaotic motion which appears as a bounded chaotic sea,

(2) regular motion associated with the inner islands which are in resonance with the field frequency and are embedded inside the chaotic sea,

(3) regular motion associated with the outer regular regions in the classical phase space.

The Schrödinger equation is obtained when $\hat{p} = -i\hbar_{\text{eff}}\partial/\partial q$. The effective Planck constant is defined as

$$[\hat{p}, q] = i\hbar_{\text{eff}}, \quad (14)$$

where

$$\hbar_{\text{eff}} = \frac{4\hbar k_L^2}{M\delta\omega}. \quad (15)$$

M is the molecular weight of the atoms (cesium in the AUSTIN experiment and sodium in the NIST experiment), k_L is the mean wave vector of the two standing waves, and $\delta\omega$ is the beating frequency between the two standing laser waves.

For the AUSTIN experiment $\hbar_{\text{eff}}=2.08$, whereas for the NIST experiment $\hbar_{\text{eff}}=0.8011$. Note that in the two cases different scaling transformations have been used and it does not necessarily imply that the AUSTIN experiment is more quantum than the NIST experiment. Since the time period in NIST experiment is $T=2\pi$ and in AUSTIN experiment it is equal to $T=1$, there is a difference in convention in defining effective Planck constant. To convert AUSTIN to NIST units one must divide $\hbar_{\text{eff}}(\text{AUSTIN})=2.08$ by 2π . Therefore, the effective Planck constant is smaller in the AUSTIN experiment than in the NIST experiment. However, what really matters is not the value of \hbar_{eff} but the ratio between the area of the relevant inner regular islands in the classical phase space and \hbar_{eff} [3]. As this ratio gets smaller values the system is more in the quantum regime.

The bound chaotic sea in the classical phase space can support $S_{\text{chaotic}}/2\pi\hbar_{\text{eff}}$ quantum states where S_{chaotic} is the area of the bound chaotic region in the classical phase space.

Similarly, the number of quantum regular states are defined as the area of the regular inner island in the classical Poincaré surface of section divided by $2\pi\hbar_{\text{eff}}$. In both cases it is less than 1. In the AUSTIN experiment this ratio is equal to 0.16 whereas in the NIST experiment it is equal to 0.06. Therefore, the NIST experiment is more quantum than the AUSTIN experiment. Indeed there is a clear fingerprint of the inner regular island in the 3D representation of the quantum global phase space entropy for the AUSTIN experiment (this type of quantum representation of the classical phase space will be discussed later in Sec. V). However, in both cases the systems are not in the semiclassical regime. Nevertheless as we will show here there is a clear fingerprint of the classical chaotic dynamics in the quantum dynamics.

Let us now briefly describe how the Floquet-Bloch are calculated. In our problem of periodically driven atoms in one-dimensional optical lattice, $H(q, t) = H(q+a, t+T)$, where $a=2\pi$ is the dimensionless scaled lattice constant and T is the dimensionless scaled time period. The Floquet-Bloch solutions of the time dependent Schrödinger equations with time periodic Hamiltonian which is defined in Eq. (10) are given by

$$\Phi \equiv \Psi_{\alpha, k}^{F-B}(q, t) = e^{ikq} e^{-iE_{\alpha, k}^{QE} t} \Phi_{\alpha}^{(k)}(q, t), \quad (16)$$

where $E_{\alpha, k}^{QE}$ and

$$\Phi_{\alpha}^{(k)}(q, t) = \sum_m C_{m, \alpha}^{(k)}(t) e^{imq} = \Phi_{\alpha}^{(k)}(q + 2\pi, t + T), \quad (17)$$

are correspondingly the eigenvalues and the eigenfunctions of the Floquet k th Bloch quasimomentum operator, $\mathcal{H}_k(q, t)$,

$$\mathcal{H}_k(q, t) \Phi_{\alpha}^{(k)}(q, t) = E_{\alpha, k}^{QE} \Phi_{\alpha}^{(k)}(q, t), \quad (18)$$

where $\mathcal{H}_k(q, t)$ is given by

$$\mathcal{H}_k(q, t) = -i\hbar_{\text{eff}} \frac{\partial}{\partial t} - \frac{\hbar_{\text{eff}}^2}{2} \frac{(\partial - ik)^2}{\partial q^2} - \gamma[\theta + \cos(t)]\cos(q). \quad (19)$$

In order to reduce the numerical effort of the computations of the Floquet-Bloch quasienergy states rather than solving Eq. (18) the Bloch quasienergy spectrum $E_{\alpha, k}^{QE}$, i.e., the eigenvalues of \mathcal{H}_k , and the corresponding quasienergy wave functions, $\Phi_{\alpha}^{(k)}(q, t)$, were calculated in a two-step procedure. In the first step of the calculations the time evolution matrix for the k th Bloch quasimomentum Hamiltonian has been constructed, using 100 free rotor basis functions, i.e., $[\exp(imq)]$, where $-50 \leq m \leq +50$ and $-1/2 \leq k \leq +1/2$ when the transformed optical lattice constant is equal to 2π . The eigenvalues and the eigenfunctions of the k th time evolution matrix provide correspondingly the quasienergies, $E_{\alpha, k}^{QE}$ and quasienergy Floquet-Bloch states at $t=0$, $\Phi_{\alpha}^{(k)}(q, t=0)$. Namely, using the (t, t') formalism [16,17],

$$\exp[-i\mathcal{H}_k(q, t')T/\hbar_{\text{eff}}] \Big|_{t'=T} \Phi_{\alpha}^{(k)}(q, t=0) = \lambda_{\alpha, k}^{QE} \Phi_{\alpha}^{(k)}(q, t=0), \quad (20)$$

where

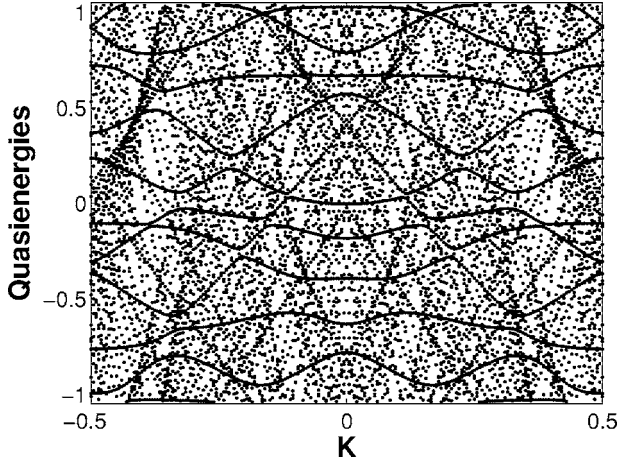


FIG. 3. The QE as a function of the Bloch quasimomentum for the NIST experiment, showing the breakdown of the Bloch-band structure of the static one-dimensional optical lattice which is associated with the classical chaotic dynamics.

$$\lambda_{\alpha,k}^{QE} = \exp(-iE_{\alpha,k}^{QE}T/\hbar_{\text{eff}}). \quad (21)$$

In the second step of the calculations the $\Phi_{\alpha}^{(k)}(q, t=0)$ states were propagated to provide $\Phi_{\alpha}^{(k)}(q, t)$ at any time $0 \leq t \leq T$,

$$\Phi_{\alpha}^{(k)}(q, t) = [\lambda_{\alpha,k}^{QE}]^{-i/T} \exp(-i\mathcal{H}_k(q, t')/t/\hbar_{\text{eff}})|_{t'=t} \Phi_{\alpha}^{(k)}(q, t=0), \quad (22)$$

where

$$\Phi_{\alpha}^{(k)}(q, t) = \Phi_{\alpha}^{(k)}(q, t+T). \quad (23)$$

The quasienergies $E_{\alpha,k}^{QE} = [i\hbar_{\text{eff}} \ln \lambda_{\alpha,k}^{QE}]/T$ are obtained as modulo of $2\pi\hbar_{\text{eff}}/T$. A simple way to get the quasienergies which are associated with the calculated quasienergy Floquet-Bloch solutions is by the calculations of the expectation values of $\mathcal{H}_k(q, t)$,

$$E_{\alpha,k}^{QE} = \langle\langle \Phi_{\alpha}^{(k)}(q, t) | \mathcal{H}_k(q, t) | \Phi_{\alpha}^{(k)}(q, t) \rangle\rangle, \quad (24)$$

where $\langle\langle \dots \rangle\rangle$ stands for integration over time and space, i.e., $T^{-1} \int_0^T dt \int_{-\infty}^{+\infty} dq \dots$. The numerical advantage of this approach over the direct diagonalization of the Floquet-Bloch operator is explained elsewhere [16,17]. Our results for the Floquet-Bloch quasienergy bands are presented in Fig. 3 showing the rich symmetry structure of the spectra of our system. The spectrum presented in Fig. 3 is in complete agreement with Fig. 10 in Ref. [14] where Hensinger and his co-workers published the results they obtained from simulation calculations for the NIST experiment. See also Fig. 5 in Ref. [15], where Mouchet *et al.* studied the large fluctuations of the tunneling transition probabilities for the same problem studied here (only different potential parameters). The chaotic dynamics are reflected in the breakdown of the Bloch-band structure which is obtained for the static one-dimensional optical lattices. The fact that very small change in the quasimomentum change dramatically the values of many quasienergies plays an important role in the suppression of the time periodic oscillations of the mean momentum. This phenomena will be discussed in detail in Sec. V.

How are quantum chaotic and regular states defined? In what sense are they associated with the classical dynamics?

In 1994 Moiseyev, Korsch, and Mirbach [9] proposed the following criterion. The chaotic states are associated with the quasi-energy states (i.e., Floquet-Bloch solutions) that provides about the same maximal values of the Shannon entropy, $S_{\alpha,k}$, and about the same expectation values of the field free Hamiltonian, $\langle H_0 \rangle_{\alpha,k}$. The $\langle H_0 \rangle_{\alpha,k}$ is define as

$$\langle H_0 \rangle_{\alpha,k} = \langle\langle \Psi_{\alpha,k}^{FB}(t=0) | H_0 | \Psi_{\alpha,k}^{FB}(t=0) \rangle\rangle, \quad (25)$$

where H_0 is the field free Hamiltonian, and $\langle\langle \dots \rangle\rangle$ stands for integration over time and space, i.e., $T^{-1} \int_0^T dt \int_{-\infty}^{+\infty} dq \dots$. The Floquet-Bloch quasienergy states, $\Psi_{\alpha,k}^{FB}(q, t)$ are numerically calculated using the linear variational principle, where the basis set expansion given in Eq. (17) is truncated. That is, m in Eq. (17) is varied from $-M/2$ to $+(M-1)/2$ rather than from $-\infty$ to $+\infty$. The variational parameters are $C_{m,\alpha}^{(k)}$ as defined in Eq. (17). Consequently, the field free expectation values are given by

$$\langle H_0 \rangle_{\alpha,k} = \sum_m |C_{m,\alpha}^{(k)}(0)|^2 \frac{(\hbar_{\text{eff}} m)^2}{2}. \quad (26)$$

Using the definition of the Shannon entropy as given in Ref. [9] and by using the basis set expansion of the Floquet-Bloch quasienergy states as presented in Eq. (17), the Shannon entropy is expressed in terms of the computed linear variational parameters,

$$S_{\alpha,k} = - \sum_j p_{j,\alpha}^{(k)} \ln p_{j,\alpha}^{(k)} = - \sum_m |C_{m,\alpha}^{(k)}(0)|^2 \ln |C_{m,\alpha}^{(k)}(0)|^2, \quad (27)$$

where $p_{j,\alpha}$ is the occupation probability of the j th field-free state by the α th quasienergy Floquet-Bloch state.

The Shannon entropy is a basis set dependent concept. However, as it was discussed in Refs. [4,9] the Shannon entropy helps to identify the regular and chaotic quantum states when the field-free eigenfunctions are chosen as a basis set. The chaotic quasienergy quantum states, which its corresponding Husimi representations show that they are embedded in the chaotic sea of the classical phase space, get about the same values of the Shannon entropy and of $\langle H_0 \rangle_{\alpha,k}$. Whereas, the regular quantum quasienergy states get different values of $\langle H_0 \rangle_{\alpha,k}$ and smaller values of the Shannon entropy. The use of the Shannon entropy to identify the regular and chaotic quantum states is illustrated in the results presented for periodically driven rotor in Ref. [4] and in our results presented here in Fig. 4(a) where \hbar_{eff} gets a sufficiently small value of 0.14 (to approach the semiclassical limit). The question is how the picture presented in Fig. 4(a) is affected by increasing the value of \hbar_{eff} to the experimental values.

In Fig. 4 the expectation values of the field free energies vs. the entropy [respectively, defined in Eqs. (26) and (27)] for the Bloch quasimomentum $k=0$ are presented. As one can see from the results presented in Fig. 4 although the experimental values of \hbar_{eff} are relatively large, a quite similar behavior of $\langle H_0 \rangle_{\alpha,k=0}$ vs. $S_{\alpha,k=0}$ is obtained. However, as

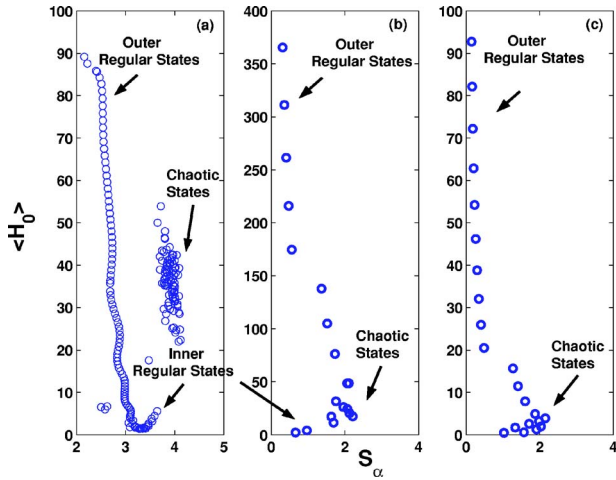


FIG. 4. (Color online) $\langle H_0 \rangle$ vs Shannon's entropy for different QE Floquet states. (a) For the AUSTIN experiment with $\hbar=0.14$. (b) For the AUSTIN parameters with $\hbar=2.08$. (c) For the NIST parameters with $\hbar=0.8011$. The states are numbered and ordered following the values of $\langle H_0 \rangle$.

one can see from the results presented in Figs. 4(b) and 4(c) the chaotic states are not entirely separated from the inner regular quasienergy states when \hbar_{eff} gets either the AUSTIN or the NIST experimental values.

The distinction between the inner-regular and the chaotic quasienergy states is possible only in the semiclassical calculations where \hbar_{eff} is sufficiently small. In the NIST and AUSTIN experiments it is hard to distinguish between the states that are associated with the inner-regular and those which are associated with the chaotic quasienergy state. The interesting result is that based on the Shannon entropy calculations one can clearly distinguish between the quasienergy states which are associated with the outer-regular island and those which are associated with the mixed chaotic-inner-regular states. The Husimi representations of the quasienergy states which were identified, with the help of the Shannon entropy calculations, as mixed chaotic-inner-regular states are presented in Sec. IV. The Husimi representations enable us to get more detailed insight information. The Husimi representations enable us to find out which one of the quasienergy states which are embedded in the mixed chaotic-inner-regular states are exponentially localized at the inner-regular islands, or in the classical chaotic region in the classical phase space, or both in the chaotic region and at the inner-regular islands.

In the NIST experiment, as one can see from the comparison of the results presented in Figs. 4(a)–4(c), the distinction between the inner-regular and the chaotic quasienergy states is slightly better than in the AUSTIN experiment. In the NIST experiment, where it has been already shown that the dynamics is controlled by a two-state mechanism [1,6,14], the inner-regular Floquet-Bloch quasienergy states are well separated from the chaotic ones, than in AUSTIN experiment (where the dynamics is controlled by a three-state mechanism [2,6]). In the case of the AUSTIN and NIST experiments the effective of the Planck constant is large enough to “push” the inner-regular quasienergy states towards the cha-

otic states, as shown in Fig. 4(c). In a way, it reminds the situation in a static problem where two potential wells are separated by a potential barrier. In the static problem the energy splitting between the two almost degenerated states that are localized inside the two potential wells, is increased as the Planck constant is increased. Eventually, for a sufficiently large value of the Planck constant, one of the two relevant energy levels, is “pushed” above the potential barrier and interacts with the delocalized states which are embedded above the potential barrier. A similar behavior is presented here for the time periodic potential where the analog to the two static potential wells are the two regular islands in the classical phase space and the analog to the static barrier is the dynamical barrier. This analogy has been made before and it is known [1,2,6]. Here we emphasize on the ability to assign the quantum quasienergy states as regular and chaotic states although the effective Planck constant is so large that the inner-regular islands cannot support even a single quasienergy state. The results presented here show very clearly that the $\langle H_0 \rangle$ vs the Shannon entropy plots (that enable the classification of the quantum states as regular and chaotic states) which were obtained for the NIST and AUSTIN experiment are very similar to the plot obtained for a similar problem where the Planck constant is small and the semiclassical approximation holds.

It is shown here that there is one-to-one correspondence between the number of the quasienergy states that are involved in the NIST and AUSTIN experiments and the ability to classify all computed quasienergy states as regular and chaotic ones. As we will show later in Sec. IV also in the case where 3-state mechanism controls the dynamics as in the AUSTIN experiment, the ability to distinguish between inner-regular and chaotic state is obtained by calculating linear combinations of the two quasienergy states which interact as the effective Planck constant is increased and one of the inner-regular quasienergy state is “pushed” to the chaotic region.

III. FINGERPRINTS OF THE MIXED REGULAR-CHAOTIC STRUCTURE OF THE CLASSICAL PHASE SPACE IN THE COLD ATOM MANIPULATION EXPERIMENTS

Here, we address ourselves to the following question: How can the quantum correspondence to the stroboscopic synoptic Poincaré classical phase space be calculated? The answer to this question will enable us to find out whether the classical chaotic dynamics is reflected in the quantum system although the effective Planck constant is large (too large to support even a single quasienergy state in the inner-regular islands).

Let us first provide a brief account of the classical phase space entropy. Following Ref. [22] the classical phase space entropy is given by

$$S_{\text{cl}}(p, q) = - \int \rho_{\text{cl}}(p_0, q_0; p, q) \ln \rho_{\text{cl}}(p_0, q_0; p, q) dp_0 dq_0, \quad (28)$$

where the classical density probability, $\rho_{\text{cl}}(p_0, q_0; p, q)$, can be obtained following Ref. [18] when the classical phase

space is divided into \mathcal{N} cells centered at discrete points denoted by (p_i, q_i) . Then, one defines $\rho_{cl}(p_0(i), q_0(i); p(j), q(j))$ as the time averaged probability for a trajectory initially located in cell $(p_0(i), q_0(i))$ to visit cell $(p(j), q(j))$. Let us briefly explain how we calculate the classical density probability. First we carry out classical trajectory calculations when initially the classical particle is centered at the i th cell which has been defined above. As time passes we count how

many visits this classical particle had in the center of the j th cell. Let us assume that during the long propagation time, i.e., $0 \leq t \leq N_t T$ where T is the period of the time dependent field and N_t gets a very large value, there were all together $N(i \rightarrow j)$ visits in the j th cell. The classical density probability is given by $\rho_{cl}(p_0(i), q_0(i); p(j), q(j)) = N(i \rightarrow j) / \sum_{j=1}^{\mathcal{N}} N(i \rightarrow j)$.

The classical phase-space entropy is approximated by

$$S_{cl}(p(j), q(j)) \sim - \sum_i \rho_{cl}(p_0(i), q_0(i); p(j), q(j)) \ln \rho_{cl}(p_0(i), q_0(i); p(j), q(j)), \quad (29)$$

where

$$\sum_j \rho_{cl}(p_0(i), q_0(i); p(j), q(j)) = 1, \quad (30)$$

for any point, $(p(j), q(j))$ in the classical phase space. In Figs. 5(a) and 5(b) the results of our calculations of $S_{cl}(p(j), q(j))$ for the NIST and the AUSTIN experiments are presented. A comparison between Figs. 1, 2, and 5 shows that in both experiments there is a remarkable similarity between the contour plots obtained for the NIST and the AUSTIN experiments from the classical phase-space entropy calculations and from the classical calculations of the stroboscopic Poincaré sections of the classical phase space.

In 1995 Mirbach and Korsch [13] defined a quantum phase space entropy which directly reflects the global classical dynamical properties of the system. The Mirbach-Korsch quantum phase-space entropy, $S_{M-K}(p, q, t=nT)$, is explained

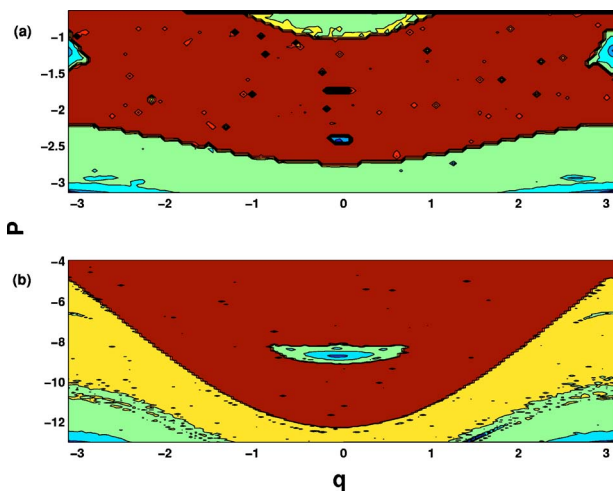


FIG. 5. (Color online) The classical global phase-space entropy (a) for the NIST parameters (b) AUSTIN experiments. The similarity to the stroboscopic Poincaré sections of the classical phase spaces for the NIST and AUSTIN experiments presented in Figs. 1 and 2 is remarkable.

below for the sake of clarity and coherency of our representation of the results for the NIST and AUSTIN experiments [13,18].

The first step in the calculations of the generalized Mirbach-Korsch entropy the quasienergy Floquet-Bloch states are projected on the coherent Gaussian wave packets that uniformly cover all available classical phase space. It should be realized that in our case the coherent wave packet should satisfy the following condition:

$$\Psi_{q_0, p_0}^{\text{coherent}}(q) = \Psi_{q_0, p_0}^{\text{coherent}}(q + a), \quad (31)$$

where a is the lattice constant which for the transformed Hamiltonian is equal to 2π .

The conventional definition of a coherent wave packet is given by [19,20]

$$\Psi_{q_0, p_0}^{\text{coherent}}(q) = \mathcal{N} e^{-[(q - q_0)^2 / 2\Omega \hbar_{\text{eff}}] + (ip_0 q / \hbar_{\text{eff}})}. \quad (32)$$

However, this conventional definition does not hold in our case since the necessary condition given in Eq. (31) does not hold. Averbukh, Moiseyev, Mirbach, and Korsch addressed themselves to this question for a continuously driven rotor [4]. A problem which is very similar to the continuously driven cold atoms in 1D optical lattice. They followed the presentation of a coherent wave packet for a rotor (or any other periodic potential as in our studied case) suggested a long time ago by Chang and Shi [21]. As explained in Ref. [21] the coherent Gaussian wave packets for spatial periodic system are expanded in $[\exp(imq)]$ orthonormal basis set,

$$\Psi_{q_0, p_0}^G(q) = \sum_{m=-\infty}^{\infty} G_m(p_0, q_0) e^{imq}, \quad (33)$$

where the expansion coefficients $\{G_m(p_0, q_0)\}$ are given by

$$G_m(p_0, q_0) = \mathcal{N} e^{-[(\hbar_{\text{eff}} m - p_0)^2 / 2\Omega \hbar_{\text{eff}}] + imq_0}, \quad (34)$$

$\Omega / 2\hbar_{\text{eff}}$ is the width of the Gaussian distributed states, and \mathcal{N} is a normalization factor. Ω is a squeezing parameter that can be adopted to the particular case. In our calculations $\Omega = 0.5$.

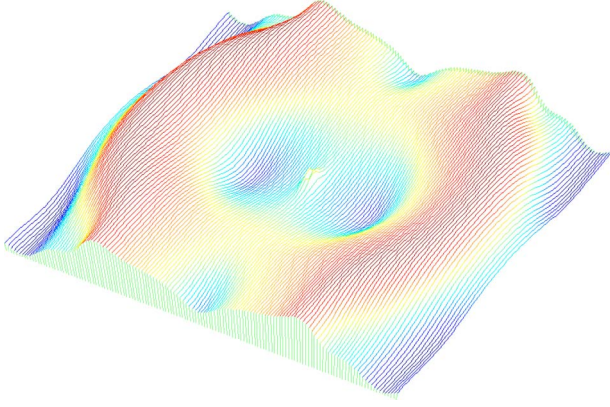


FIG. 6. (Color online) 3D representation of the quantum global phase-space entropy for NIST experiment showing clearly that a low entropy region (island) is obtained at the large inner regular as appears in the classical surface of section presented in Fig. 1.

In the second step of the calculations of the Mirbach-Korsch quantum phase-space entropy, the Husimi representations of the Floquet-Bloch quasienergy states (eigenfunctions of the Floquet operator) are calculated. The importance of the phase-space formulation is in helping us to visually represent complicated dynamics by drawing contour plots of the quantum phase-space distribution function. Let us briefly explain the need for the Husimi representations.

The phase space representation of quantum system is established through the use of quantum distribution functions such as the Wigner and the Husimi distribution functions. It allows one to describe quantum phenomena using classical language. Thus, providing useful insights in the field of quantum-classical correspondence. The Husimi distribution function is often chosen when dealing with quantum systems which are classically chaotic since it gets positive values only (unlike the Wigner distribution) and has a very simple smooth form. The Husimi is calculated by projecting the Floquet state on a coherent Gaussian wave packet as defined in Eq. (33). Later we will use this special definition of the Husimi representation of a quasienergy state to define the initial wave packet in our calculations of the oscillating mean momentum as a function of time.

Consequently, the Husimi representation of the α th Floquet-Bloch quasienergy state for the k th Bloch quasimomentum, is given by

$$\Gamma_{\alpha,k}(p_0, q_0) = \mathcal{N}^2 \left| \sum_m C_{m,\alpha}^{(k)}(0) e^{[(\hbar_{\text{eff}}^m - p_0)^2 / 2\Omega \hbar_{\text{eff}}] - i q_0 m} \right|^2, \quad (35)$$

where $C_{m,\alpha}^{(k)}$ are the linear variational coefficients as defined in Eq. (17). The Husimi distributions should be normalized such that the summation over all quasienergy states yields no information such that

$$\sum_{\alpha} \Gamma_{\alpha,k}(p_0, q_0) = 1 \quad (36)$$

for each phase-space point (p_0, q_0) .

By now we are ready for the representation of the next step in the calculations of the Mirbach-Korsch generalized quantum phase-space entropy. The quantum phase-space density kernel is calculated for the k th quasimomentum Bloch state,

$$\rho^{(k)}(p_0, q_0; p, q) = \sum_{\alpha} \Gamma_{\alpha,k}(p_0, q_0) \Gamma_{\alpha,k}(p, q). \quad (37)$$

The quantum phase-space density kernel, $\rho^{(k)}(p_0, q_0; p, q)$, provides the probability for the quantum particle which is associated with the k th quasimomentum Bloch state, to get from one point in the classical phase space to another one. The reason is simple. $\Gamma_{\alpha,k}(p_0, q_0)$ is the probability of the quantum particle associated with the (α, k) Bloch state to be at (p_0, q_0) . $\Gamma_{\alpha,k}(p, q)$ is the probability of the quantum particle associated with the (α, k) Bloch state to be at (p, q) . The product $\Gamma_{\alpha,k}(p_0, q_0) \Gamma_{\alpha,k}(p, q)$ provides the probability to get from one point to another one in the classical phase space when the quantum particle is in the (α, k) Bloch state. The summation over α in Eq. (37) provides the desired result. For a proof see Ref. [13].

In the last step of the calculations the Mirbach-Korsch quantum phase-space entropy is calculated for the k th quasimomentum value,

$$S_{MK}^{(k)}(p, q) = - \int \rho^{(k)}(p_0, q_0; p, q) \ln \rho^{(k)}(p_0, q_0; p, q) dp_0 dq_0. \quad (38)$$

Although the extension of the Mirbach-Korsch approach to cold atoms in 1D optical lattices seems to require the integration over all values of k such that,

$$S_{QM}(p, q) = \frac{1}{a} \int_{k=-\pi/a}^{k=+\pi/a} S_{MK}^{(k)}(p, q) dk. \quad (39)$$

in order to simplify the calculations we have calculated the Mirbach-Korsch quantum phase-space entropy for the $k=0$ quasimomentum value.

In Fig. 6 and in Fig. 7 we present the quantum phase-space entropy $S_{MK}^{(k=0)}(p, q)$ shown for the NIST and AUSTIN experiments. Let us first discuss the results obtained for the NIST experiment. Although the effective Planck's constant is large the overall picture presented in Fig. 6 is very similar to the stroboscopic Poincaré section of the classical phase space for the NIST experiment which is shown in Fig. 1. At the bounded chaotic "sea" in the classical phase space the quantum phase space entropy gets the largest values. In the region in classical phase space which is associated with the inner regular island (see Fig. 1) the quantum phase space entropy gets the smallest values (see Fig. 6). Note however that this is not the inner regular island which is associated with the dynamical tunneling experiment. The effective Planck constant is too large to enable us to explore the inner-regular island at which the initial state has been localized in NIST experiments, from the quantum phase-space entropy calculations.

The quantum phase-space entropy calculations for AUSTIN experiments shown in Fig. 7 clearly indicates on

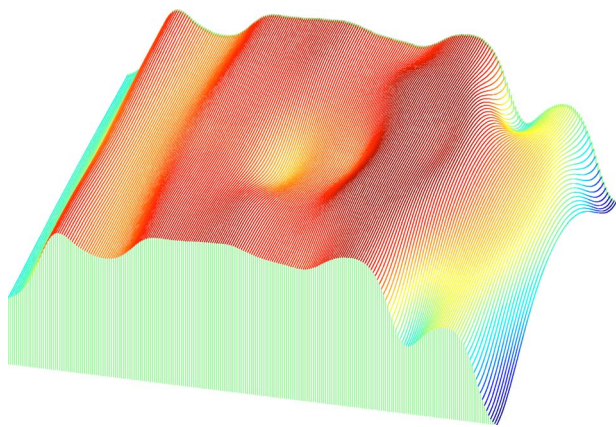


FIG. 7. (Color online) 3D representation of the quantum global phase-space entropy for AUSTIN experiment showing clearly that a low entropy region (island) is obtained at the inner regular as appears in the classical surface of section presented in Fig. 2. This inner-regular island is associated with the dynamical tunneling phenomena.

the presence of the inner-regular island as shown in Fig. 2 which is associated with the dynamical tunneling experiment.

We can summarize this section by saying that both in NIST and AUSTIN experiments the effective Planck's constant is too large to provide a detailed structure of the mixed regular-chaotic phase space through the calculations of the Mirbach-Korsch quantum phase-space entropy. However, the fact that the overall mixed regular and/or chaotic structure of the classical phase space is obtained from the quantum calculations is amazing.

IV. HUSIMI REPRESENTATIONS OF THE REGULAR AND CHAOTIC FLOQUET-BLOCH QUASIENERGY STATES IN THE COLD ATOM EXPERIMENTS

As it has been stressed in Sec. II both NIST and AUSTIN experiments are associated with the same dimensionless effective Hamiltonian. The difference between the two experiments is in the values of the dimensionless effective Hamiltonian's parameters, as are defined in Eq. (10). Since by varying these parameters (equivalent to the variation of the effective Planck's constant) one can control the dynamical tunneling mechanism we will restrict ourselves in this section to the AUSTIN's parameters. However, by varying the effective Planck's constant for the AUSTIN experiment a transition from the 3-state dynamics to the 2-state dynamics (as in NIST experiment) is obtained.

From the results presented in Fig. 4(c) one can clearly distinguish between three types of solutions. A "cluster" of 5–6 quasienergy Floquet-Bloch states which all provide about the same value of $\langle H_0 \rangle$, and about the same maximal value of $\langle S \rangle$. These are the chaotic states that their Husimi representations are embedded inside the chaotic sea in the classical phase space (presented in Fig. 2). [In Fig. 9 the Husimi distributions of a chaotic state for different values of \hbar_{eff} (labelled by $|3_a\rangle$ and $|3_b\rangle$) are presented for the AUSTIN experiment.]

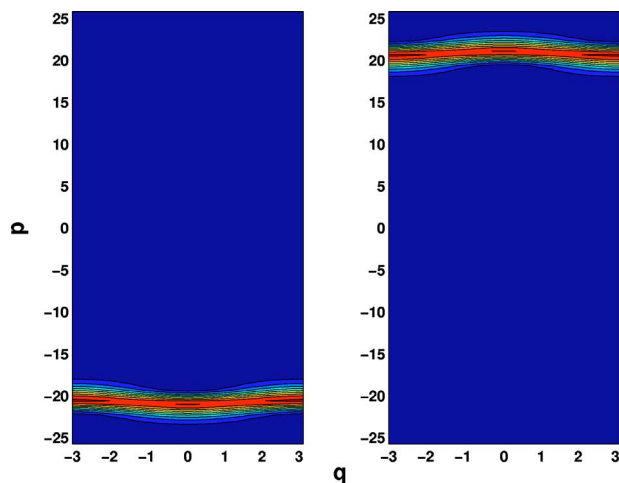


FIG. 8. (Color online) The Husimi representation of an outer state. This state is associated with the outer trajectories of the classical phase space.

A series of seven quasienergy Floquet-Bloch states that are associated with very different values of $\langle H_0 \rangle$ but all provide small values of the Shannon entropy are shown in Fig. 4 for the AUSTIN experiment. The Husimi distribution plots of these states show that they are embedded in the outer-regular region in the classical phase space. These states are the outer-regular quasienergy states. See, for example, Fig. 8 where the Husimi distributions of two almost degenerated outer-regular quasienergy states are presented. Compare the results presented in Fig. 8 with the classical phase space given in Fig. 2. All the other quasienergy states provide about the same values of $\langle H_0 \rangle$, but are associated with different Shannon entropies which are smaller than the values obtained for the chaotic states. These are quasienergy Floquet-Bloch states which are referred to as inner-regular quasienergy states. A comparison between the results obtained for a driven planar rotor and presented in Ref. [4] and the results presented here for the AUSTIN experiments clearly show that due to the large value of the effective Planck constant, the inner-regular states associated with AUSTIN experiment are "pushed" toward the direction of the chaotic states. Husimi representations of the two inner-regular quasienergy states obtained for AUSTIN experiment parameters $\hbar_{\text{eff}}=2.08$ (see Fig. 9) show that one quasienergy state [denoted in Fig. 9 by $|1_b(\hbar_{\text{eff}}=2.08)\rangle$] is exponentially localized at the inner-regular islands embedded inside the chaotic sea (see the presentation of the Poincaré surface of section in Fig. 2) whereas the other one, denoted by $|2_b(\hbar_{\text{eff}}=2.08)\rangle$ is localized at the inner-regular island and also in the chaotic region in the classical phase space. As discussed by Averbukh, Osovski, and Moiseyev in Ref. [6], by varying the experimental conditions to reduce the value of \hbar_{eff} to the value of $\hbar_{\text{eff}}=1.9$ the two quasienergy states are exponentially localized at the two regular islands. Indeed the Husimi representations of the two inner-regular quasienergy states which are shown in Fig. 9 confirm this numerical observation.

By slightly varying the AUSTIN experimental parameters to provide $\hbar_{\text{eff}}=1.9$, the 2-state dynamics as in the case of the

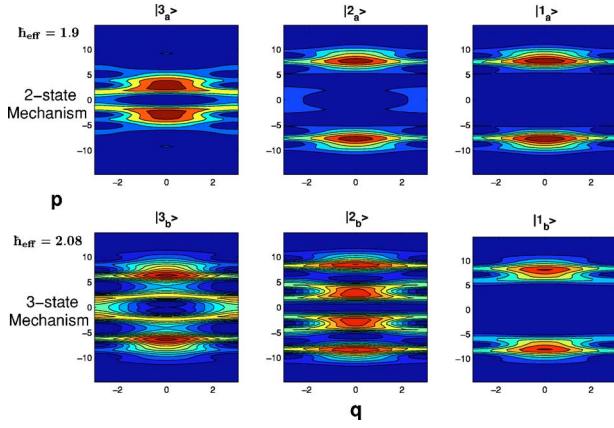


FIG. 9. (Color online) The Husimi representation of the same three QE Floquet-Bloch ($k=0$) states in different effective Planck's constant. When $\hbar_{\text{eff}}=1.9$ the tunneling mechanism is a two states mechanism, i.e., the $|1_a\rangle$ and $|2_a\rangle$ states are populated by the initial wave packet and state $|3_a\rangle$ does not participate in the process. When $\hbar_{\text{eff}}=2.08$ the tunneling mechanism is that of three states and all of the states shown take part in the dynamical tunneling phenomena due to the fact that the third state now has a part in the regular island.

NIST experiment would be obtained. However, as discussed in Ref. [6] also in AUSTIN experiment where $\hbar_{\text{eff}}=2.08$ and 3-quasienergy-state dynamics is involved, a linear combination given by

$$\frac{|1_b(\hbar_{\text{eff}}=2.08)\rangle + |2_b(\hbar_{\text{eff}}=2.08)\rangle}{\sqrt{2}} \pm |3_b(\hbar_{\text{eff}}=2.08)\rangle \quad (40)$$

provide two wave packets which are localized in one of the two inner-regular islands. See the results presented in Fig. 10 where the two linear combinations of the inner-regular quasienergy states are presented for $\hbar_{\text{eff}}=2.08$. As one can

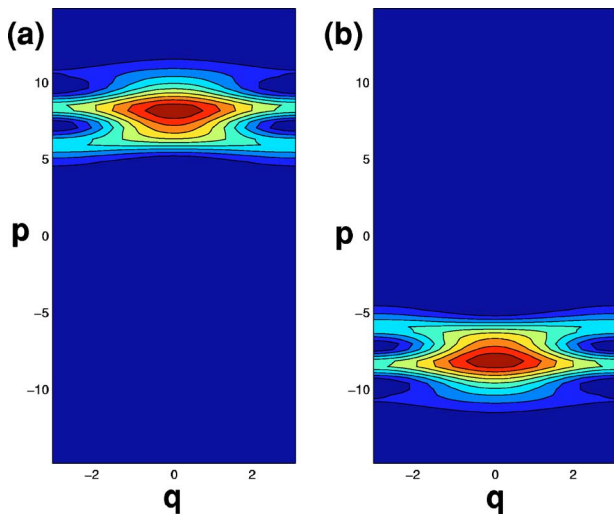


FIG. 10. (Color online) The Husimi representation of a linear combination of $|1_b\rangle$, $|2_b\rangle$, and $|3_b\rangle$ for the AUSTIN experiment.

see they are localized at the inner-regular islands at $\pm p=8.1$ and $q=0$.

We have shown in this section that in spite of the large values of the effective Planck constants the quasienergy Floquet-Bloch states can be assigned as quasichaotic, outer-regular, and inner-regular quantum states.

V. THE FINGERPRINT OF THE CHAOTIC DYNAMICS THROUGH THE AMPLITUDE'S DECAY OF THE OSCILLATORY MEASURED TIME DEPENDENT MEAN MOMENTUM

Steck carried out an average over a sinc^2 distribution function of quasimomenta to get the damped oscillations of the mean momentum [23]. Here we take a very similar approach. An important point in our analysis is to keep the ability to identify the contributions of the different Floquet-Bloch quasienergy states to the mean time dependent momentum distribution. Therefore, following the arguments given in Ref. [4] and as discussed in Sec. III, the initial state is expanded in the orthonormal $[\exp(imq)]$ basis set,

$$\psi(t=0) = \left(\frac{1}{\pi\sigma}\right)^{\frac{1}{4}} \int_{-1/2}^{+1/2} dk e^{-[(k-k_0)^2/2\sigma]} e^{ikq} \sum_m G_m(p_0, q_0) e^{imq}, \quad (41)$$

where the coefficients $G_m(p_0, q_0)$ are defined as before in Eq. (34). Here we do an average over a Gaussian distribution of quasimomenta. The Gaussian width parameter, σ , determines the population of the different k -Bloch quasimomentum states by the initial wave packet. For $\sigma \rightarrow 0$ the only populated state is the k_0 -Bloch quasimomentum state, $\psi(q, t; \sigma \rightarrow 0)$. In our studies which their results are presented here $k_0=0$. By varying the value of σ we control the population probability of the k th quasimomentum Bloch-Floquet states. Note that this definition of the initial wave packet is different from the one used in Ref. [14] in simulation calculations for the NIST experiment. In Ref. [14] the initial state was the ground state of the time independent Hamiltonian where the time dependent potential has been adiabatically turned on. Our motivation to define the initial state by Eq. (41) is to be able to extract from the time dependent mean momentum contribution of a specific well defined quasimomentum component.

It is convenient to expand the initial state in the Bloch quasienergy states as defined in the Eq. (17),

$$\psi(t=0; \sigma \rightarrow 0) = \sum_m G_m e^{imq} = \sum_{\alpha} D_{\alpha}^{(k)} \Phi_{\alpha}^{(k)}(q, t=0), \quad (42)$$

where

$$D_{\alpha}^{(k)} = \sum_m (C_{m,\alpha}^{(k)}(0))^* G_m(p_0, q_0). \quad (43)$$

The time propagated wave packet at $t=Tn$ (the time period is $T=1$ in AUSTIN experiment and $T=2\pi$ in NIST experiment) is given by

$$\psi(t = Tn) = \left(\frac{1}{\pi\sigma} \right)^{\frac{1}{4}} \int_{-1/2}^{+1/2} dk e^{-k^2/2\sigma} e^{ikq} \Psi_k(t = Tn), \quad (44)$$

where

$$\Psi_k(t = Tn) = \sum_{\alpha} \exp(-i\epsilon_{\alpha,k}^{QE} Tn / \hbar_{\text{eff}}) D_{\alpha}^{(k)} \Phi_{\alpha}^{(k)}(q, t = 0). \quad (45)$$

Note that following Eq. (42) at $t=0$ $\Psi_k(t=0)$ is independent of the value of k . Only during the propagation in time the different Bloch states, $\Psi_k(t=Tn)$ become k -dependent. Nevertheless when $\sigma \neq 0$ even at $t=0$ different k -Bloch quasimomentum states are populated. The projection of the α k th Bloch QE state on $\Psi_k(n)$ is given by

$$W_{\alpha,k}(t = nT) = |W_{\alpha,k}(n)| e^{i\gamma_{\alpha,k} 2\pi n} = \exp\left(-i \frac{Tn \epsilon_{\alpha,k}^{QE}}{\hbar_{\text{eff}}}\right) D_{\alpha}^{(k)}. \quad (46)$$

The scaled momentum at $n=0, 1, 2, \dots$ time periods is given by

$$\begin{aligned} \langle P(t = nT) \rangle &= \hbar_{\text{eff}} \int_{-1/2}^{+1/2} dk e^{-k^2/\sigma} \sum_{\alpha, \alpha'} W_{\alpha',k}^*(t = nT) W_{\alpha,k}(t) \\ &= nT \sum_m (m+k) C_{\alpha',m}^{(k)*} C_{\alpha,m}^{(k)}. \end{aligned} \quad (47)$$

The decay of the oscillations of the mean momentum does not reflect the disordered dynamics. Even when the phase factor changes with driving period regularly but significantly, the decay of the oscillations of $\langle p(t) \rangle$ should look similar albeit the dynamics look quite differently. See, for example, the stochastic dynamics for integrable systems in Ref. [24]. The question in our case is whether small changes in σ [see definition in Eq. (42)] can lead to significant changes in the time-dependent phase factors. In the cold atom experiments carried out in NIST and in AUSTIN the answer is that the extremely strong dramatic effect of very small changes of the quasimomentum values which are populated by the initial wave packet (i.e., change the value of σ), on the short-time dynamics [i.e., the decay of the amplitude of the oscillations of $\langle p(t) \rangle$] results from the breakdown of the Bloch-band structure which is associated with the classical chaotic dynamics. Let us explain this important point in some more detail. For regular systems a small change in the population of the quasimomentum states results in a small change of the quasienergy values. Since the quasienergies determine the time-dependent phase factors as defined in Eq. (46), it is clear that small changes in the populated quasienergies cannot lead to a strong effect on the short-time dynamical behavior. However, when due to the classical chaotic dynamics the small change of the value of the quasimomentum provides large changes in the values of the quasienergies, a strong effect on the short-time dynamics is obtained.

In Fig. 11 we show that the initial wave packet (WP) indeed populate in NIST experiment two different QE Floquet-Bloch states (associated with the quasimomentum $k=0$) whereas in AUSTIN experiment three states are populated by the initial WP.

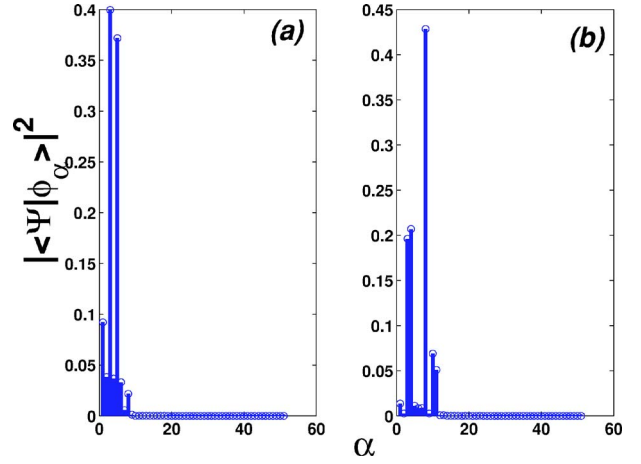


FIG. 11. (Color online) The population of the different QE Floquet-Bloch ($k=0$) states. (a) For the NIST experiment showing that only two states are populated by the initial WP. (b) For the AUSTIN experiment showing that three states are populated by the initial WP.

The decay of the tunneling is clearly shown in Fig. 12 for various values of σ for the AUSTIN experiment. As one can see the system is very sensitive to the width of the distribution in k . For the range of σ from 0 to 10^{-4} the influence is hardly notable. However, for $\sigma=3 \times 10^{-4}$ the decay is already noticeable and as σ is increased the decay is faster.

In Fig. 13 we present the complex weight factors $W_{\alpha,k}$ as function of n (i.e., time $t=nT$ where $n=0, 10$). As one can see as time passes the population probability amplitude to the Bloch QE states are randomly distributed in the complex plane. It leads to a random phase distribution of the probability amplitude from 0 to 2π . The random phase factor, $\exp(-iTn \epsilon_{\alpha,k}^{QE} / \hbar_{\text{eff}})$ results from the population of chaotic quasi-energy states which are associated with the broken Bloch-band structure as shown for example in Fig. 3. In AUSTIN experiment the initial atomic state is superimposed

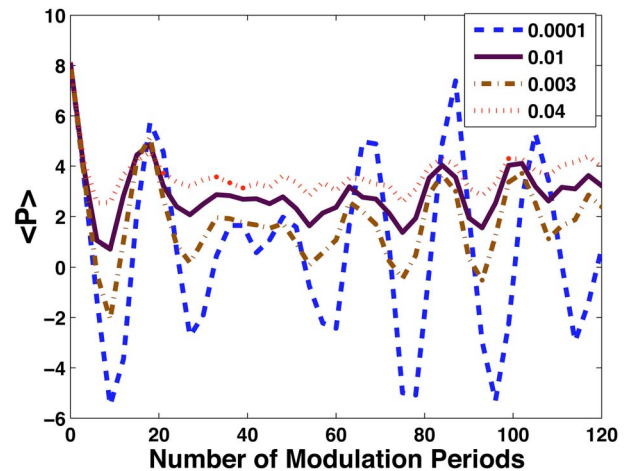


FIG. 12. (Color online) The mean momentum as a function of modulation periods, for various values of σ when considering all the Bloch quasimomentum states in the first Brillouin zone, $-a/2\pi \leq k \leq a/2\pi$ for the AUSTIN experiment.

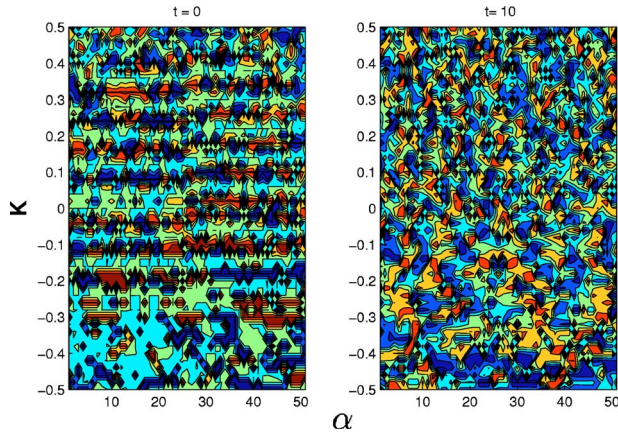


FIG. 13. (Color online) The phases of the weight factors are shown in different time modulation periods for the AUSTIN experiment. As one can see when time passes they are more uniformly distributed.

on the upper island in three different regions in the classical phase space (see Fig.1 in Ref. [2]), whereas in our quantum calculations the initial wave packet is centered at the upper island. Therefore, we cannot make a detailed comparison between the theoretical results and the experimental one. However, a comparison between our results presented in Fig. 12 and Fig. 1 and 12 in Ref. [2] shows the qualitative agreement of our theoretical results with the experimental ones.

We have applied the same treatment to the experiment done by the NIST's group. Similar results were obtained as shown in Fig. 14. The conclusion is clear. The random distribution in the complex plane of the probability amplitudes associated with the nonzero quasimomentum components leads to the decay of the amplitude of the oscillations in the time dependent mean momentum measurements. As time passes and the random distribution in the complex plane of the probability amplitudes (so called weight factors in our derivation) is developed, the decay of the amplitude of the oscillations of the mean momentum is developed as well. In Fig. 15 our theoretical results are compared with the experi-

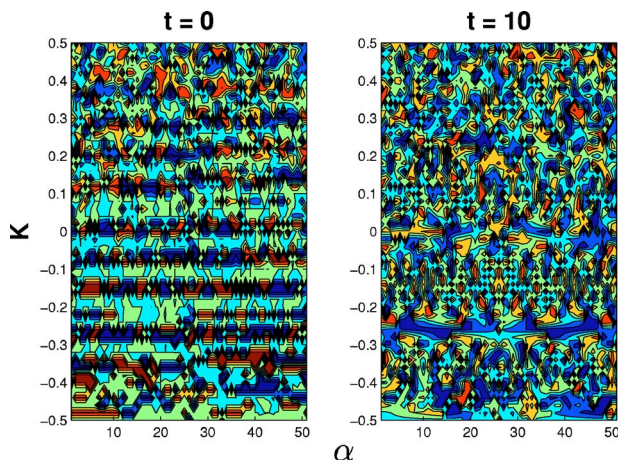


FIG. 14. (Color online) The phases of the weight factors are shown in different time for the NIST experiment. As one can see when time passes they are more uniformly distributed.

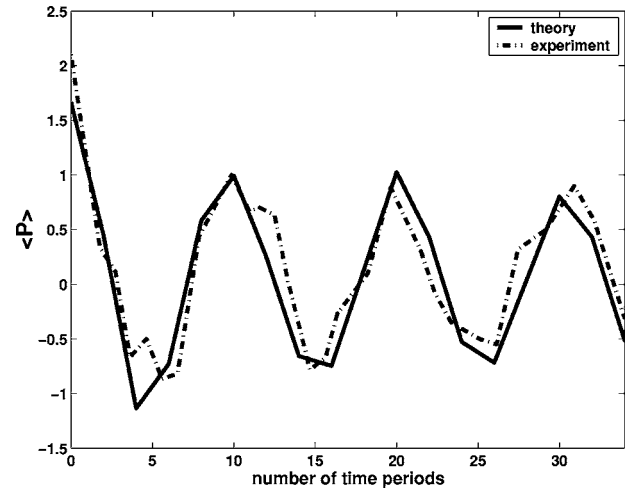


FIG. 15. Our theoretical results vs. the experimental results as obtained in NIST [1]. The theoretical results were obtained when $\sigma=0.002$ [see Eq. (42) in the text] which implies that 99.9% of the cold atoms were initially prepared to be in the $k=0$ quasimomentum

mental ones as obtained in the NIST experiment. A remarkable agreement has been obtained when $\sigma=0.002$ [see the definition in Eq. (42)] and therefore most of the atoms (i.e., 99.9%) are in the $k=0$ quasimomentum Floquet states.

VI. CONCLUDING REMARKS

In both NIST and AUSTIN experiments, the value of \hbar_{eff} does not approach the semiclassical limit. In spite of this fact the calculations of the Shannon entropy, as well as those of the calculations of the Mirbach-Korsch quantum phase-space entropy, clearly show the fingerprints of the mixed classical phase-space structure.

The Shannon entropy plots presented in Fig. 4 enable us to distinguish between the regular states and the chaotic ones. The corresponding Husimi representations of the regular states are exponentially localized in the regular regions in the classical phase space. In particular those which are associated with the outer regular regions as shown, for example, in Fig. 8. The corresponding Husimi representations of the chaotic states are embedded in the classical chaotic sea (see, for example, $|3_a\rangle$ and $|3_b\rangle$ in Fig. 9).

The correspondence between the global shape of the Mirbach-Korsch quantum phase-space entropy plots presented in Figs. 6 and 7 and the stroboscopic Poincaré surface of section of the classical phase space for the NIST and AUSTIN experiments (see Figs. 1 and 2) is quite amazing in spite of the absence of fine details in the quantum ones. The bounded classical chaotic sea is associated with the region where the quantum phase space entropy gets large and about the same values. The chaotic sea is presented as a high plateau in the quantum phase-space entropy plots. For the NIST experimental parameters the large inner-regular island centered at $q_0=0$, $p_0=0$ is clearly seen in the quantum phase-space entropy plot of Fig. 6. The smaller inner-regular islands are not seen in the quantum phase-space entropy plot. However, for the AUSTIN experimental parameters the

inner-regular island which is associated with the dynamical tunneling phenomena is clearly seen in the quantum phase-space entropy plot in Fig. 7.

The time dependent Husimi representations clearly show that the periodic oscillations of the mean momentum of the cold atoms, $\langle P(t) \rangle$, results from the transitions from one regular island to another through the chaotic sea. The decay of the amplitude of the oscillating $\langle P(t) \rangle$ in the experiments is shown to result from the random phase distribution of the population probability amplitudes of the different quasimomentum Bloch-Floquet states (see, for example, Fig. 12). The random phases are accumulated as the wave packet gets through the classical chaotic region. The phase of the overlapping integral between the k th Bloch component of the propagated wave packet and the k th Bloch QE α th Floquet state at $t=nT$ is shown to be equal to $\exp(-iTn\epsilon_{\alpha,k}^{QE})$. Since the quasienergies as function of the Bloch quasimomentum show clearly both regular and chaotic bands (see Fig. 3), it is expected that the accumulation of random phases will be obtained as the initial wave packet populates different quasimomentum states. Indeed as we have shown here the high population of the zero quasimomentum Bloch state (more than 99%) by the initially prepared wave packet, plays a crucial role in the dynamical tunneling measurements. Namely, if in the NIST and AUSTIN experiments the $k=0$ quasimomentum Floquet states would not be the most dominant ones, the oscillatory behavior of the mean momentum would not have been observed. This theoretical result is in harmony with the experimental observation (see Fig. 15). The fact that the wave packet, initially centered at one of two inner-regular islands, while it oscillates between the two

regular islands through the chaotic sea accumulates a random phase is another fingerprint of chaos in quantum dynamics. To the best of our knowledge this kind of fingerprint of chaos in quantum mechanics (associated with the breakdown of the Bloch-band structure of the static one-dimensional optical lattices) has been first measured in the NIST and AUSTIN experiments. For regular systems small change in the value of the quasimomentum makes a small change in the values of the quasienergies. Therefore, for regular systems the effect of small changes in the quasimomentum on the short time dynamics is negligible. Only when for classical chaotic dynamics, a very small change in the quasimomentum [i.e., $\sigma = 0.002$ in Eq. (42)] is associated with large changes in values of the quasienergy (which determine the time dependent phase factors) and thereby provide a large effect on the short time dynamics of the studied system. We expect that in measurements where the population of a single Bloch quasimomentum will be carefully varied, the correlation between the population of a single Bloch quasimomentum state and the rate of decay of the amplitude of the oscillating mean momentum will be observed. Moreover, the oscillations of the mean momentum in time, should be observed whenever more than 99% of any k th quasimomentum Bloch state is populated and not necessarily the $k=0$ Bloch state.

ACKNOWLEDGMENTS

This work was supported in part by the Israel Science Foundation (Grant No. 1152/04) and by the Fund of promotion of research at the Technion. It is our pleasure to thank Dr. Vitali Averbukh and Professor Shmuel Fishman for most helpful discussions.

-
- [1] W. K. Hensinger, H. Haffner, A. Browaeys, N. R. Heckenberg, K. Helmerson, C. McKenzie, G. J. Milburn, W. D. Phillips, S. L. Rolston, H. Rubinsztein-Dunlop, and B. Upcroft, *Nature (London)* **412**, 52 (2001).
 - [2] D. A. Steck, W. H. Oskay, and M. G. Raizen, *Science* **293**, 274 (2001).
 - [3] D. A. Steck, W. H. Oskay, and M. G. Raizen, *Phys. Rev. Lett.* **88**, 120406 (2002).
 - [4] V. Averbukh, N. Moiseyev, B. Mirbach, and H. J. Korsch, *Z. Phys. D: At., Mol. Clusters* **35**, 247 (1995).
 - [5] A. Mouchet, C. Miniatura, R. Kaiser, B. Gremaud, and D. Delande, *Phys. Rev. E* **64**, 016221 (2001).
 - [6] V. Averbukh, S. Osovski, and N. Moiseyev, *Phys. Rev. Lett.* **89**, 253201 (2002).
 - [7] E. J. Heller, *Phys. Rev. Lett.* **53**, 1515 (1984).
 - [8] L. Kaplan and E. J. Heller, *Phys. Rev. E* **59**, 6609 (1999).
 - [9] N. Moiseyev, H.J. Korsch, and B. Mirbach, *Z. Phys. D: At., Mol. Clusters* **29**, 125 (1994).
 - [10] A. Wehrl, *Rev. Mod. Phys.* **50**, 221 (1978).
 - [11] S. Kohler, R. Utermann, P. Hänggi, and T. Dittrich, *Phys. Rev. E* **58**, 7219 (1998).
 - [12] I. Vorobeichik, M. Orenstein, and N. Moiseyev, *IEEE J. Quantum Electron.* **34**, 1772 (1998).
 - [13] B. Mirbach and H. J. Korsch, *Phys. Rev. Lett.* **75**, 362 (1995).
 - [14] W.K. Hensinger, A. Mouchet, P.S. Julienne, D. Delande, N. R. Heckenberg, and H. Rubinsztein-Dunlop, *Phys. Rev. A* **70**, 013408 (2004).
 - [15] A. Mouchet, C. Miniatura, R. Kaiser, B. Gremaud, and D. Delande, *Phys. Rev. E* **64**, 016221 (2001).
 - [16] U. Peskin and N. Moiseyev, *J. Chem. Phys.* **99**, 4590 (1993).
 - [17] N. Moiseyev, *Comments At. Nucl. Phys.* **31**, 87 (1995).
 - [18] B. Mirbach and H.J. Korsch, *Ann. Phys. (N.Y.)* **265**, 80 (1998).
 - [19] J.R. Klauder and B.-S. Skagerstam, *Coherent States Applications in Physics and Mathematical Physics* (World Scientific, Singapore, 1985).
 - [20] C. Cohen-Tannoudji, B. Diu, and F. Lalo, *Quantum Mechanics* (Wiley-Interscience, New York, 1977).
 - [21] S.-J. Chang and K.-J. Shi, *Phys. Rev. A* **34**, 7 (1986).
 - [22] K. Takahashi, *Prog. Theor. Phys. Suppl.* **98**, 109 (1989).
 - [23] D. A. Steck, Ph.D. thesis, p. 215; <http://www.ph.utexas.edu/quantopt/disses.html#phd>
 - [24] N. Moiseyev, *J. Phys. Chem.* **87**, 3420 (1983).